Abstract. The spatial association of narrow band metric radio spikes with type III bursts is analyzed. The analysis addresses the question of a possible causal relation between the spike emission and the acceleration of the energetic electrons causing the type III burst. The spikes are identified by the Phoenix-2 spectrometer (ETH Zurich) from survey solar observations in the frequency range from 220 MHz to 530 MHz. Simultaneous spatial information was provided by the Nançay Radioheliograph (NRH) at several frequencies. Five events were selected showing spikes at one or two and type III bursts at two or more Nançay frequencies. The 3–dimensional geometry of the single events has been reconstructed by applying different coronal density models. As a working hypothesis it is assumed that emission at the plasma frequency or its harmonic is the responsible radiation process for the spikes as well as for the type III bursts. It has been found that the spike source location is consistent with the backward extrapolation of the trajectory of the type III bursts, tracing a magnetic field line. In one of the analyzed events, type III bursts with two different trajectories originating from the same spike source could be identified. These findings support the hypothesis that narrow band metric spikes are closely related to the acceleration region.

Key words: Sun: flares – Sun: particle emission – Sun: radio radiation

A&A manuscript no.
(will be inserted by hand later)

Your thesaurus codes are:
missing; you have not inserted them

ASTRONOMY AND ASTROPHYSICS
April 1, 2001

Spatial analysis of solar type III events associated with narrow band spikes at metric wavelengths

G. Paesold[1,2], A.O. Benz[1], K.-L. Klein[3], and N. Vilmer[3]

[1] Institute of Astronomy, ETH Zentrum, CH-8092 Zurich, Switzerland
[2] Paul Scherrer Institute, Würenlingen und Villigen, CH-5232 Villigen PSI, Switzerland
[3] Observatoire de Paris, Section de Meudon, DASOP & CNRS UMR 8645, 92195 Meudon, France

Received 12 February 2001/ Accepted 19 February 2001

1. Introduction

Millisecond narrow band radio spikes are structures in the radio spectrum of the Sun forming a distinct class of flare emission. The term 'narrow band, millisecond spikes' refers to short (few tens of ms) and narrow band (few percent of the center frequency) peaks in the radio spectrogram. They can be observed in the range of 0.3 to 8 GHz and occur mainly during the impulsive phase of a solar flare. Since the spike emission is often associated with enhanced hard X-ray emission (Benz & Kane 1986; Güdel et al. 1991; Aschwanden & Güdel 1992) it is suspected that spikes are closely related to the actual process of energy release in solar flares.
The short duration and the narrow bandwidth suggest a small source size and therefore a high brightness temperature (up to 10^{15} K). Only a coherent mechanism can account for the emission but none of the proposed mechanisms is generally accepted. Proposed emission mechanisms are the electron cyclotron maser (e.g. Holman, Eichler & Kundu 1980, Melrose & Dulk 1982, Aschwanden 1990, Robinson 1991) and upper hybrid or z-mode instabilities combined with wave-wave coupling (e.g. Zheleznyakov & Zaitsev 1975, Vlahos et al. 1983, Tajima et al. 1990 and Güdel & Wentzel 1993).
A subclass of spikes originally found at metric wavelengths correlates with type III bursts (Benz et al. 1982). They occur in clusters usually at frequencies slightly higher than the start frequency of the type III burst and are located in a dynamic spectrogram at the intersection of the extrapolated type III and the spike frequency. Although they may be slightly shifted in time (in a positive or negative direction) they significantly correlate with the extrapolated type III burst (Benz et al. 1996). Since the spike location in the spectrogram is close to the extrapolated type III burst it is a reasonable assumption that spike and type III radiations are emitted at the same characteristic frequency.
This type of radio emission has been called 'metric spikes' in the literature (e.g. Güdel & Zlobec 1991) and it is still unclear whether the spikes in the metric and the decimetric range belong to the same class of events.
Previously published spatially resolved observations of metric spike events (Krucker et al. 1995; Krucker et al. 1997) found the spike sources at high altitudes and suggest a model of energy release taking place in or close to the spike sources. Escaping beams of electrons cause the type III emission. Thus a scenario is conceivable in which the spikes may be a direct signature of the accelerator.
Using two-dimensional, spatially resolved data from the Nançay Radioheliograph (NRH), it is possible to reconstruct the spatial configuration of the event and the relative position of the spike source with respect to the type III trajectory. The main purpose of this work is to test whether the geometry of the events supports the picture mentioned above.

Send offprint requests to: G. Paesold
Correspondence to: gpaesold@astro.phys.ethz.ch

2. Instruments

2.1. The Phoenix-2 spectrometer

Since 1998 the Phoenix-2 spectrometer operated by the ETH Zurich has been continuously recording radio data from sunrise to sunset. The intensity and polarization are digitally measured by the frequency-agile receiver in the range from 0.1-4.0 GHz at a time resolution of 500 μs for single channel measurements. The receiver consists of 4000 channels at 1, 3 or 10 MHz bandwidth, from which a reduced number can be freely selected. A full description of the instrument can be found in Messmer et al. (1999). The data used herein were recorded at a bandwidth of 1 MHz and a time resolution of 100 ms in the frequency range from 220 to 550 MHz, chosen in collaboration with the Nançay Radioheliograph.

2.2. The Nançay Radioheliograph (NRH)

In July 1996 the Meudon Observatory began daily observations with the improved 2D imaging radioheliograph in Nançay (France). The instrument is described by Kerdraon & Delouis (1996). Five frequencies in the range from

150-450 MHz can be observed simultaneously at a maximum number of 200 images per second. The antennas are organized in two perpendicular arrays and digitally correlated on 576 channels resulting in measurements of Stokes I and V. The observing bandwidth is 700 kHz.
Data were taken with a frequency configuration of 164.0, 236.6, 327.0, 410.5, 432.0 MHz at a mean time resolution of 125 ms.
For older data the NRH provides one-dimensional scans of the corona at five frequencies, with both its east-west and north-south branches (The Radioheliograph Group 1993). The integration time was 1 s. The NRH then observed at 164, 236.6, 327, 408 and 435 MHz.

3. Observation and method

Data from observations of Phoenix-2 were used to identify type III events associated with metric spike emission. The choice of events was restricted by the observing frequencies of Nançay. At least one frequency was required to locate the spike emission, and the type III emission was required to be visible at least in two frequencies. The following four events were found in the recent data:

99/09/27: In the time range from 09:53.8 to 09:57.2 UT a type III burst group occurred and was accompanied by a cluster of metric spikes in the frequency range 300 to 370 MHz.

00/05/29: Type III burst group in the range from 220 - 420 MHz and metric spike emission from 390 to 430 MHz in the time range from 12:25.00 to 12:29.80 UT.

00/06/21: Metric spikes in the frequency range from 340 MHz to 450 MHz, accompanied by a type III burst group from 220 MHz to 450 MHz. The event time is 10:12.4-10:12.5 UT.

00/06/22: Type III burst group in the range from 220 MHz to 510 MHz, whereas the metric spikes are located between 400-420 MHz at the beginning of the event and between 430-500 MHz later on. The whole event lasts from 13:41.5 to 13:44.5 UT.

In addition, three separate events on 92/08/18, already published in Krucker et al. (1997) using only VLA observations at 333 MHz have been investigated using data from the previous heliograph in Nançay. The events show metric spikes in the frequency range from 310 MHz to 360 MHz and type III activity from around 300 MHz down to below 40 MHz. The time ranges for the events are 13:43:50 to 13:44:10 UT, 14:01:47 to 14:02:00 UT and 14:14:35 to 14:14:40 UT, respectively.

3.1. Phoenix-2 observations

The dynamic spectrum from 220 MHz to 530 MHz of the analyzed part of the 00/06/22 event is shown in Fig. 1 (top). In the first half of the the event (13:41:40 to about 13:42:08 UT) the metric spike emission is mainly located in the range from 370 MHz to 470 MHz. At lower frequencies the drifting structures of type III emission can be seen. In the second half, the spike emission is shifted to higher frequencies (430 MHz to 510 MHz).
In the middle panel of Fig. 1 a selected light curve at 432.0 MHz observed by the Phoenix-2 spectrometer is displayed. The data were recorded with a sampling period of 100 ms and an integration time of 0.5 ms. According to Güdel & Benz (1990) the expected mean time duration of a single spike event at 432.0 MHz is 0.062 ± 0.004 s. Therefore the single spike events are not resolved in time. Following Messmer & Benz (1999), the minimum bandwidth of spikes is given by $\sim 0.4\%$ of the center frequency yielding a value of 1.73 MHz at 432.0 MHz. Although this value is close to the spectral resolution of 1 MHz of Phoenix-2, the spikes are resolved in frequency and can be well identified.
No polarization information is available from Phoenix-2 data for this event nor for the 00/06/21 and the 00/05/29 events since the spectrometer was run with a linear feed during this time.
The description of the observation mode of the old Phoenix spectrometer for the 92/08/18 event can be found in Krucker et al. (1997).

3.2. Nançay observations

The bottom panel in Fig. 1 shows the light curve at 432.0 MHz of the same event observed by NRH. The data were recorded with an integration time of 125 ms at a sampling rate of 125 ms. Since the integration time of NRH is longer than of Phoenix-2, the noise level of the dataset is lower.
The software used to analyze the 2D NRH data offers a source tracking routine that allows the user to determine location and size of a radio source in the 2D image of the Sun. The relevant source was identified from Phoenix-2 observations by simultaneously determining the flux in the NRH data and comparing it to the full sun observation of Phoenix-2 (cf. Fig. 1 middle and bottom). The size of the source is determined by fitting an ellipse with minimal perimeter at half height of the peak flux.
The error of the source centroid consists of two parts: A discretization error and a statistical error. The first one stems from the NRH data being gridded. The centroid position determined by the NRH software lies on a grid and the distance between two grid points is $\sim 0.016 R_\odot$. Hence, there is a minimal error which is given by half the diagonal of a pixel $\sim 0.011 R_\odot$.
The *statistical* uncertainty of the centroid position is given

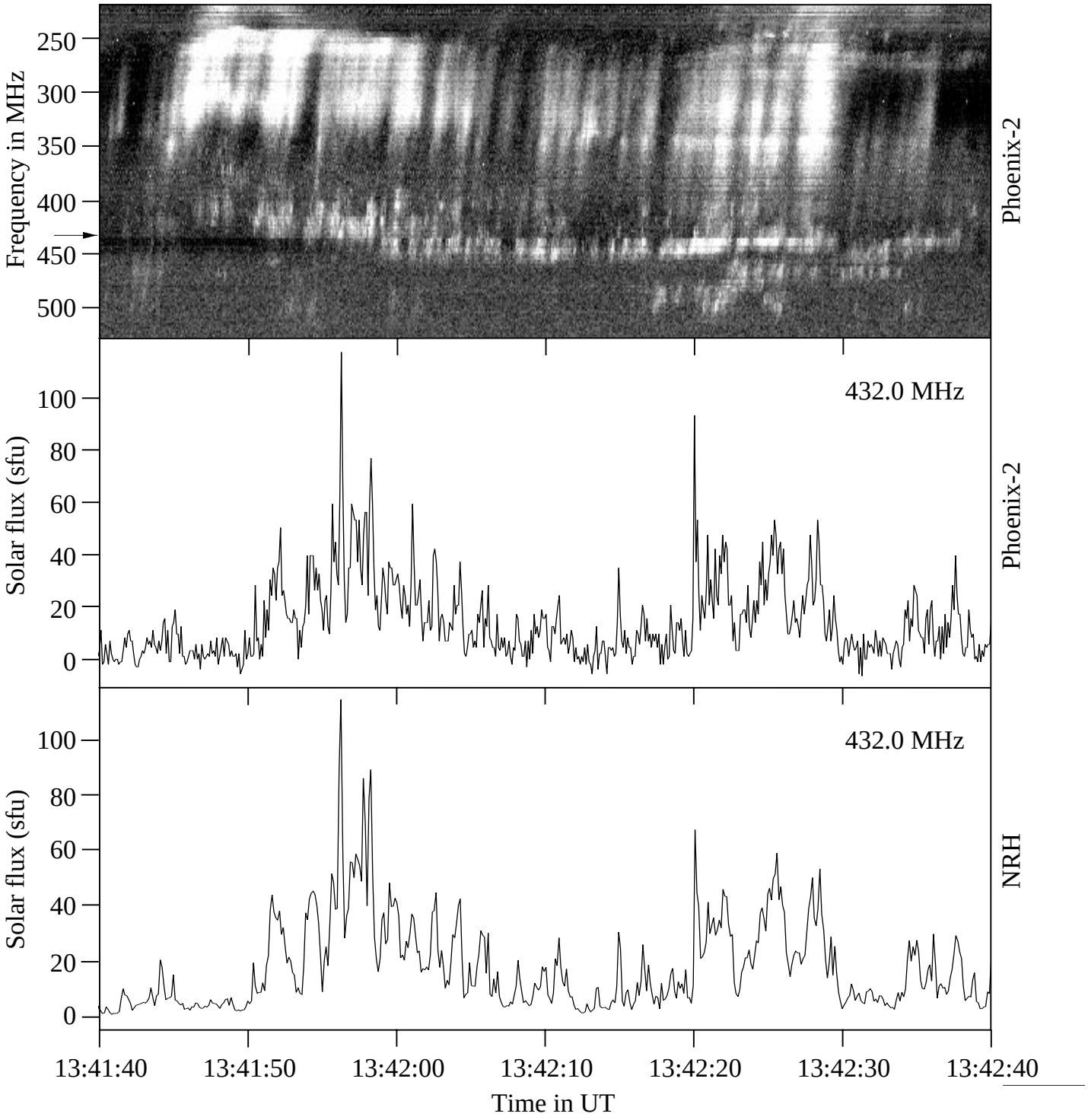

Fig. 1. Top: Spectrogram observed by Phoenix-2 on 00/06/22. White regions correspond to enhanced flux; the frequency axis is from top to bottom. **Middle:** Light curve of metric spikes recorded by the Phoenix-2 spectrometer at a single frequency (432.0 MHz). The arrow in the top panel indicates the position of 432.0 MHz. **Bottom:** NRH light curve of metric spikes at the same frequency.

by the observed radius, Φ, of the source times the noise to flux ratio. This ratio is constant according to the radiometer equation, and the resulting error Δ can be written as

$$\Delta = \frac{\sigma_{\max}}{F_{\max}}\Phi = \frac{\sigma}{F_{\rm bg}}\Phi \qquad (1)$$

where the index *max* refers to the peak values, σ is the noise level at the background and F_{bg} is the background flux. The noise can be determined from the background level at the source position before or after the event. In

most cases, the statistical error was smaller than the discretization error, thus the latter one was used. Otherwise Eq. 1 yields the error bar.
In the case of the 92/08/18 event, the integration time in the NRH data is so long that the accuracy of the centroid determination is given by the pixel size. This has been verified in the following way: 1D scans were made at 164 and 327 MHz during five observing runs on Cyg A between 6 and 31 August 1992 and analyzed in the same way as the solar data. At 164 and 327 MHz, Cyg A appears as a simple source when observed with both the east-west and north-south array. The measured centroid positions contain a random part and a slowly varying offset, which was evaluated by a polynomial fit. The analysis yields a statistical uncertainty of $\sim$ 1 pixel (error bar) for both frequency channels and a systematic offset of one pixel in the interval of hour angles corresponding to the solar observations on 92/08/18.

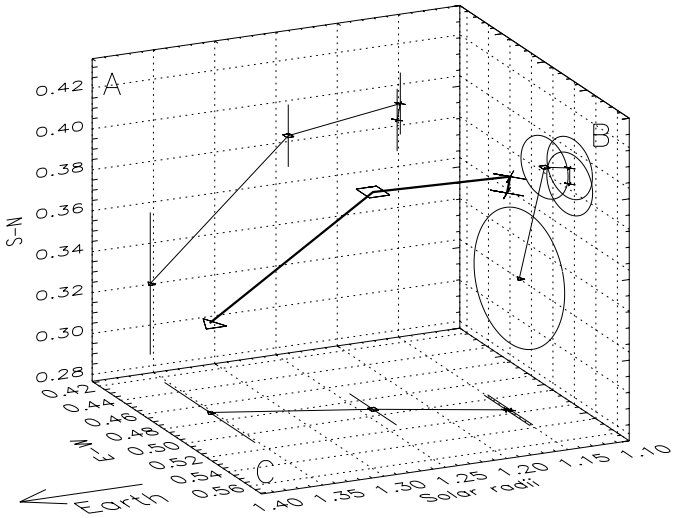

Fig. 2. 3–dimensional view of one of the bursts in the 99/09/27 event. The projection on A corresponds to the upper left panel in the plots of Figs. 3, 4 and 6, the projection on B to the upper right and the projection on C to the lower right panel.

3.3. Association of spikes and type III bursts

The identification of a single type III burst was mainly made by visual identification in the spectrogram. Only the stronger type III bursts of a group have been chosen for the analysis in order to ensure that they can be continuously traced back to the start frequency. In case of doubt the correlation function of two light curves at the relevant frequencies was computed and the burst was identified by correlation peaks. In case of more than one correlation peak, consistency with the drift rate between other frequencies was the criterion. However, it is still possible that two type III bursts with only a slight difference in drift rate crossover in the spectrogram and the associated sources do not belong to the same burst. As described in Sect. 4 the sources at each frequency of the analyzed events are very stable. Either each of the bursts in the group has a crossover with another type III on the "wrong" field line, which is not very probable, or the crossing type III burst occurs on the same field line and the source location is de facto not distinguishable from the source of the original burst.
By extrapolating the type III burst to the spike frequency, the associated spikes were identified. However, since the spikes can be slightly shifted in time with respect to the extrapolated type III burst (Benz et al. 1996), a time window of about ± 0.2 s has to be used in order to take all possible associated spikes into account. The positions of all spikes inside the time window were included in the analysis.
Simultaneous emissions at two frequencies have been admitted if two of the observed frequencies lie in the spike range.

4. Results

The results for the four recent events (99/09/27, 00/05/29, 00/06/21, 00/06/22) are presented in chronological order whereas the 92/08/18 events will be analyzed separately. In order to display three dimensional situations in two dimensions, height projections on the solar equatorial plane and the meridian plane which we define by the earth and the solar poles have been chosen for representation in Figs. 3, 4 and 6 (see Fig. 2). The upper right panel of each plot depicts the actual observations of Nançay as described in 4.1 whereas the upper left and the lower right panel result from the 3–dimensional reconstruction described in Sect. 4.3. The symbols representing the observing frequencies are chosen as follows: $\star = 432.0$ MHz, $+ = 410.5$ MHz, $\times = 327.0$ MHz, $\square = 236.6$ MHz and $\triangle = 164.0$ MHz.
The lines connecting the source centroids display how the sources are related to each other in the spectrogram. For reasons of visualization the observed source centroid positions in the 92/08/18 events have been interpolated by 3–dimensional splines to smooth curves.
The sources do not vary significantly in the course of the event for all analyzed events. Hence, for every event, one single representative burst out of the group has been plotted, although the analysis contains many more identified type III bursts.

4.1. Observation

References to Figs. 3, 4 and 6 in this section always refer to the upper right panel displaying the square shown in the overview (lower left panel).

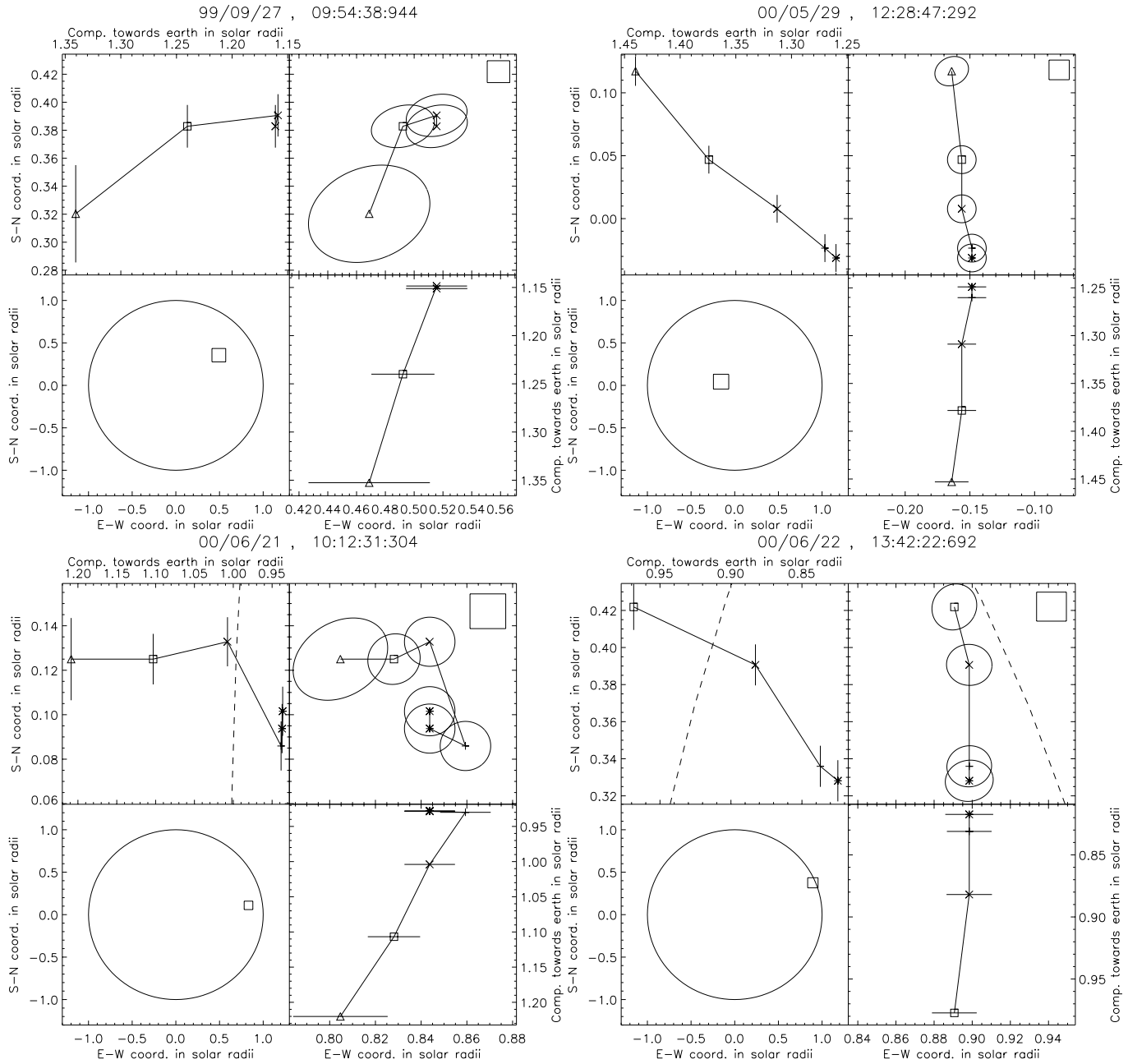

Fig. 3. A representative burst for each event is displayed. *Lower left:* global position of the event on the Sun. The small square indicates the image size presented in the *upper right* quadrant, where the positions observed by the NRH are given. The square in the upper right corner represents the grid size of the NRH image. The positional error of the source centroids are indicated by ellipses. *Upper left:* Projection of the sources on the meridian plane (view seen from an observer West of the sources). *Lower right* The sources in the projection on the equatorial plane, showing the view of an observer North of the Sun (cf. Fig. 2).

99/09/27: Five type III bursts were identified at 164.0 MHz during this event. Two of the NRH frequencies (164.0 MHz, 236.6 MHz) lie in the range of the type III bursts and one (327.0 MHz) in the spike range. The event occurred on the first quadrant of the solar disc. The source positions at each frequency vary only within the error bars, indicating a stable magnetic configuration during the event. Therefore it can be assumed that the bursts occurred practically on the same magnetic field lines. One representative burst of this group is depicted in Fig. 3 (upper left plot).

00/05/29: Three type III bursts were identified at 164.0 MHz in this group occurring between 12:28:46 and 12:28:49 UT. All five observing frequencies of NRH could be used for this event. Three frequencies (164.0 MHz, 236.6 MHz, 327.0 MHz) lie in the range of the type III emission and two (410.5 MHz, 432.0 MHz) in the spike

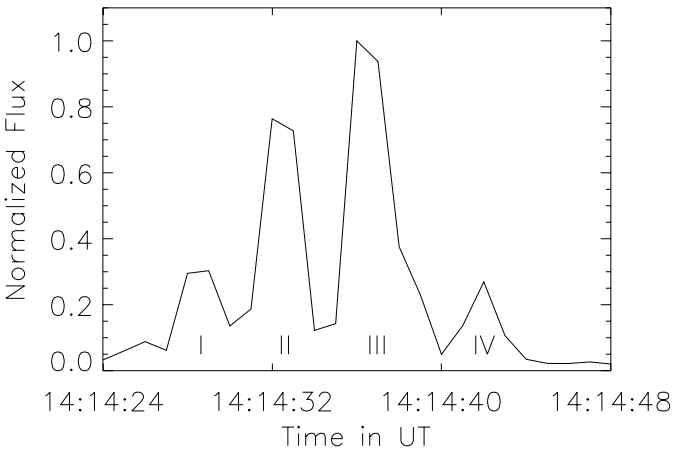

Fig. 5. Light curve of the 92/08/18 14:14 UT event at 164.0 MHz. The Roman numerals refer to the four identified type III bursts.

range. The spatial variation of the sources among the different bursts is within the error bars and therefore the three bursts are assumed to have occurred approximately on the same magnetic field line. The upper right plot in Fig. 3 displays one representative burst out of this group.

00/06/21: Between 10:12:28 and 10:12:44 UT six type III bursts were identified. Again all five frequencies of NRH could be used for the analysis. Three frequencies (164.0 MHz, 236.6 MHz, 327.0 MHz) lie in the range of the type III emission and two (410.5 MHz, 432.0 MHz) in the spike range. The event occurred close to the solar limb in the first quadrant. The sources at 164.0, 236.6, 327.0 and 410.5 MHz are stable within the error bars. The source at 432.0 MHz exhibits a larger spatial variation than observed in all other events. The type III source at 327.0 MHz is the most difficult one in the whole dataset to fit with a field line connecting the sources at all frequencies. The lower left plot in Fig. 3 displays one representative burst.

00/06/22: Three bursts out of this group have been analyzed. 236.6 MHz and 327.0 MHz lie in the type III frequency range and 410.5 MHz and 432.0 MHz lie in the spike range. The spatial variation of the sources is negligible, and as in the other events the extrapolated type III trajectory intersects the observed spike source.

4.1.1. 92/08/18 event

Three events of type III bursts with associated metric spikes were identified on 92/08/18 starting at 13:44 UT, 14:02 UT and 14:14 UT, respectively.

13:44 UT: During the first event, three type III bursts were identified at 164.0 MHz. Two more NRH frequencies could be used for the analysis: 236.6 MHz in the type III range and 327.0 MHz in the spike range.
The scattering of the source centroid positions during the event lies within the error bars for each frequency. One representative burst is displayed in Fig. 4.

14:02 UT: This event is of special interest since it exhibits simultaneous sources at 164.0 MHz at different locations. Only one type III burst could be clearly identified in the spectrogram. At 164.0 MHz two sources were found: a stronger one more to the East and a weaker one more to the West. At 236.6 MHz only one source position could be clearly identified. This position is consistent with only one of the positions at 164.0 MHz. Due to the possible close positions of the sources and the time resolution of 1 s, a weaker second source at 236.6 MHz would be difficult to detect.
At 327.0 MHz, in the spike range, one source was found. Hence, in Fig. 4 on the right, both 164.0 MHz sources have been plotted whereas only one source at 236.6 MHz is displayed. The more probable trajectory in this configuration is depicted. Nevertheless, since the disconnected 164.0 MHz source is the stronger one and is without doubt part of the event, the situation is interpreted as two type III bursts propagating on different field lines, giving evidence of electrons being injected into different coronal structures from one single spike source.

14:14 UT: The light curve at 164.0 MHz for this type III group is depicted in Fig. 5. Four bursts have been identified and labeled I-IV. Special attention has been given to this event for the following reason: Bursts I and IV occurred at a location significantly different from the position of bursts II and III. By analyzing the situation at 236.6 MHz, two sources were found with less, but still significant, spatial separation than at 164.0 MHz. At 327.0 MHz, a frequency lying in the spike range, the positions of the associated spike sources coincide.
Although the geometry is quite similar to the event at 14:02 UT, it exhibits a different situation since the bursts are consecutive and not simultaneous. Therefore, the identification and association of the sources was easier, and at every frequency the single bursts could be well identified.
The superposition of the radio centroid positions on the Yohkoh-SXT image (Fig. 6) suggests that the two electron beam trajectories inferred from the radio data correspond to magnetic field lines with different connectivities. The eastward oriented trajectory projects above loops that connect the trailing part of the active region (NOAA 7260) in the West with the leading part of an active region in the eastern hemisphere (NOAA 7264). The compact northward oriented trajectory is consistent with electron beams being guided by large-scale magnetic structures bending westward, possibly toward the leading part of AR 7260. The trailing part of AR 7260 had a complex magnetic polarity (δ spot) which produced several flares in

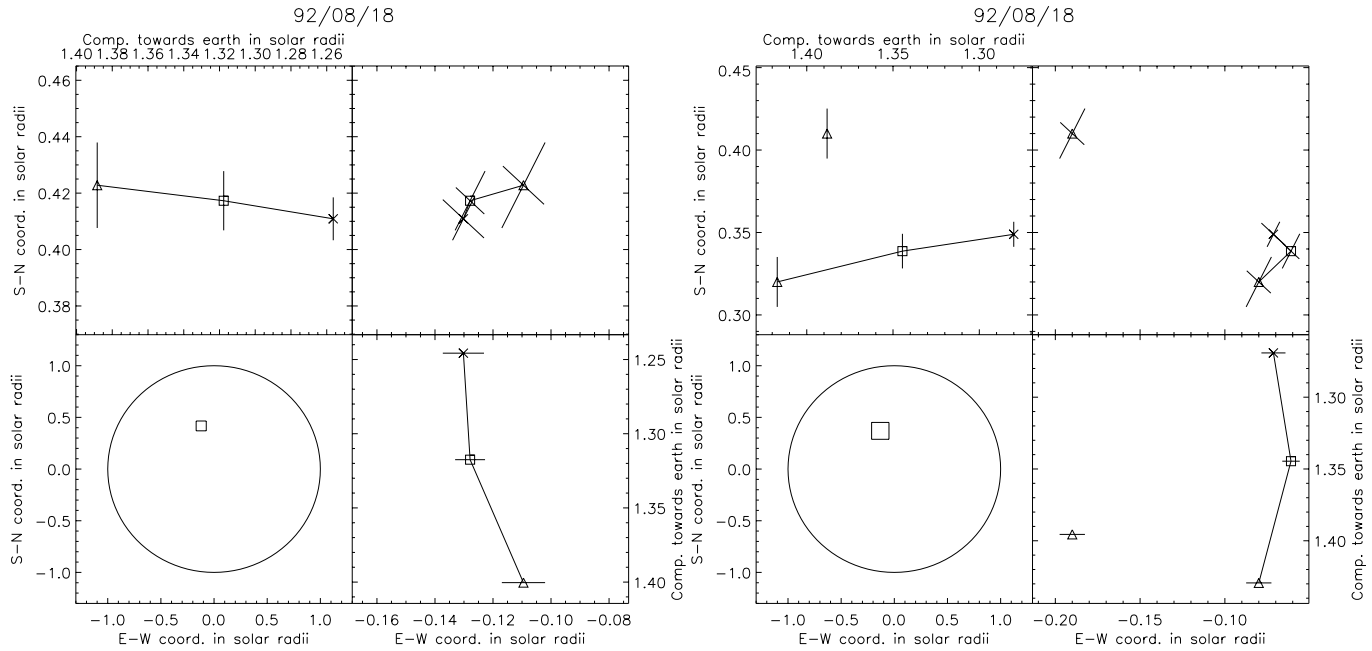

Fig. 4. Left: A representative burst from the first type III group at 13:44 UT, 92/08/18. **Right:** Burst in the second event at 14:02 UT, 92/08/18. The symbols are the same as described in the caption of Fig. 2.

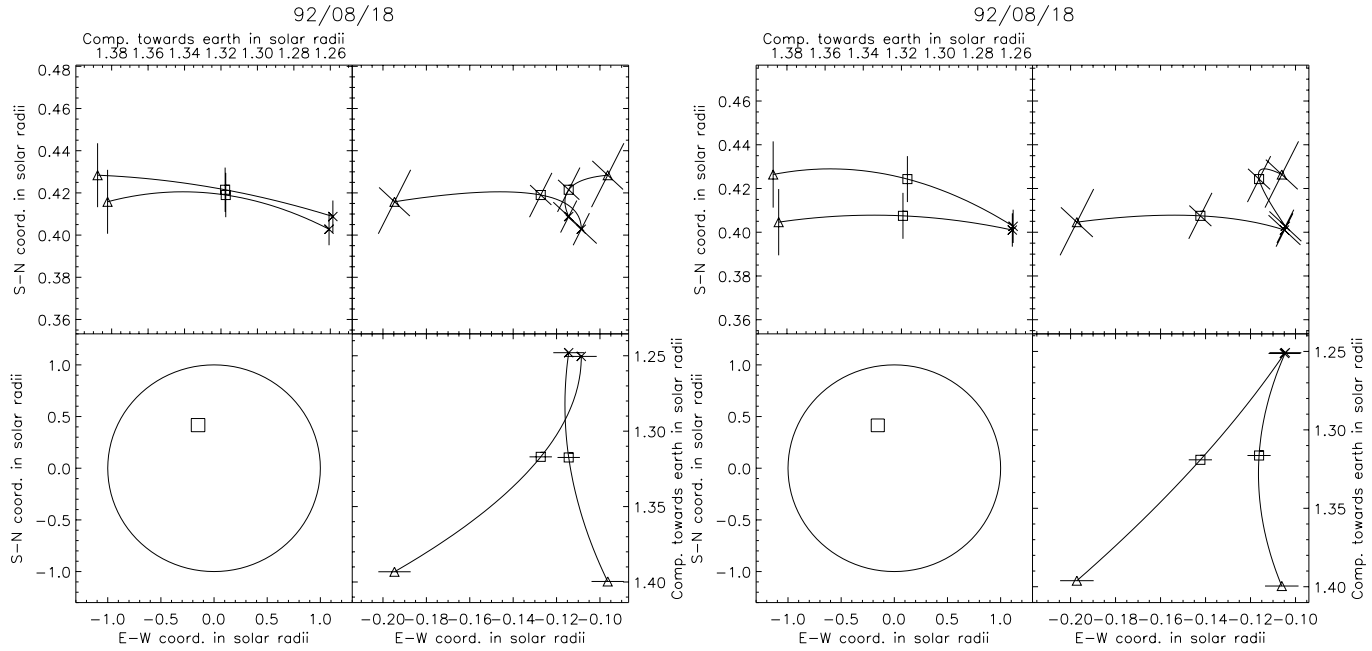

Fig. 6. Left: Reconstructed trajectories of bursts I and II of the 92/08/18 14:14 UT event. The Roman numerals refer to the first two bursts identified in Fig. 5. **Right:** Burst III and IV of the 92/08/18, 14:14 UT event. In both plots the trajectories have been 3–dimensionally spline interpolated in order to make the distinction between error bars and trajectory easier. The symbols are the same as described in the caption of Fig. 2.

August 1992 (cf. Leka et al. 1996) and is thus a plausible site for electron acceleration.

4.2. Polarization

With the exception of the limb event on 00/06/22, significant circular polarization was detected in all cases. The degree of polarization was moderate ($\sim$ 10%) for the type III emission, and much stronger (up to 90-100%) for the spikes. The sense of the polarization was the same

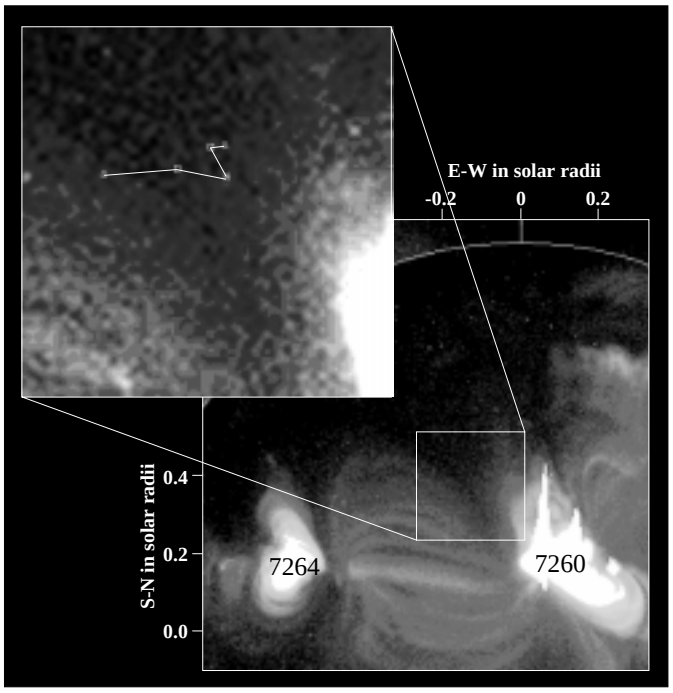

Fig. 7. Yohkoh SXT picture overlaid with radio sources. The SXT image was taken with the Al.1 filter at 16:29:07 UT. The integration time was 2.668 s. Two of the 92/08/18 event radio bursts are displayed (see also Fig. 6, right panel). The symbols are the same as described in the caption of Fig. 3

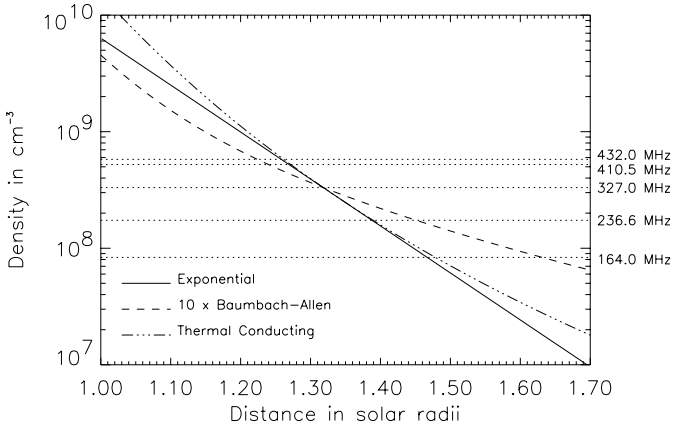

Fig. 8. Coronal density vs. distance from the Sun center. Three different models have been plotted. The scale height and reference values of density and height for the exponential and thermal conductivity model have been chosen to be $H_n = 7.5 \cdot 10^9 cm$, $n_0 = 3.36 \cdot 10^8 cm^{-3}$ and $h_0 = 2.21 \cdot 10^{10} cm$. The horizontal dotted lines indicate the densities corresponding to the observing frequencies of Nançay assuming emission at the harmonic of the plasma frequency.

for spikes and type III bursts, consistent with the results found by Benz et al. (1996) and references therein.

4.3. Spatial reconstruction

4.3.1. Coronal density models

Assuming emission either at the fundamental or harmonic of the plasma frequency, the height of the radio source can be determined from a coronal density model $n_e(h)$ via

$$\omega \approx \mathrm{a} \cdot \omega_p = \left(\frac{4\pi\, e^2\, n_e(h)}{m_e} \right)^{1/2} \quad , \tag{2}$$

where h is the height above the solar photosphere, and a is about one or two for fundamental or harmonic emission, respectively.

Three different atmospheric models have been used and compared: An exponential atmosphere, the 10×Baumbach-Allen model (Baumbach 1937; Allen 1947) and an atmosphere in hydrostatic equilibrium with thermal conductivity (Lang 1980). The latter two are given by

$$n_e^{\mathrm{BA}}(h) \;=\; 10 \cdot 1.55 \cdot 10^8 \left(\frac{h}{R_\odot} \right)^{-6} \times \\ \times \left[1 + 1.93 \left(\frac{h}{R_\odot} \right)^{-10} \right] \;\mathrm{cm}^{-3} \tag{3}$$

for the Baumbach-Allen model and

$$n_e^{\mathrm{TC}}(h) \;=\; n_0 \left(\frac{h}{h_0} \right)^{-2/7} \times \\ \times \;\exp\left[-\frac{7\, h_0}{5\, H_n} \left\{ 1 - \left(\frac{h}{h_0} \right)^{-5/7} \right\} \right] \tag{4}$$

for the thermally conducting corona. n_0 and h_0 are reference values for density and according height, H_n is the scale height, corresponding to the scale height of the exponential density model. The reference values were chosen according to observations of Trottet et al. (1982) and Suzuki & Dulk (1985). Sources at 160 MHz have been found at heights of about 0.5 solar radii above the photoshpere which is reproduced by the model under the assumption of harmonic emission. The resulting density from all three models is depicted in Fig. 8.

Although the solar corona is not expected to have a spherically symmetric density distribution, the models are considered to apply to single magnetic flux tubes which are supposed to be the type III guiding structures in the corona. Being anchored in the parent active regions, the flux tubes can exhibit curvature and significantly deviate from radiality. Nevertheless, the density within an individual flux tube can be assumed to follow a model such as described above.

The 3–dimensional position of the radio sources is assumed to be at the intersection of the line of sight and the sphere defined by the density model (Eq. 2). As all the sources were observed on the disc, there was no ambiguity. Propagation effects and their impact on the source positions are discussed in Sect. 5.

If not mentioned otherwise, the exponential density model and $a = 2$ has been used in the following. It is still con-

troversial whether structureless type III bursts (i.e. no fundamental–harmonic pairs) are emitted at the fundamental or the harmonic of the plasma frequency. This question shall not be discussed here and we refer the reader to the review of Suzuki & Dulk (1985) and references therein.
The results of the 3–dimensional reconstruction are shown in the upper left (side-view) and lower right (top-view) panels of each plot in Figs. 3, 4 and 6. The component towards Earth is the projection of the radio source's height on the axis perpendicular to the plane of the sky (cf. Fig. 2).
It is the most important result that in all cases analyzed here, the observed locations of the spikes coincide in a smooth and natural way with the expected position of radio emission at the corresponding frequencies from extrapolating the type III trajectory to lower altitudes.

5. Discussion

In the following we discuss the findings in the previous section addressing the 3D reconstruction of the bursts, including possible influence of radio wave propagation effects, and the interpretation of spikes being a signature of the accelerator.

5.1. Source locations

It is obvious that the reconstructed source locations depend on the chosen coronal density model in terms of absolute heights. The same is the case for the choice of emission at the harmonic rather than at the fundamental of the plasma frequency. However, the relative positions which are of major interest in this work are not altered by changing either the atmospheric models nor the characteristic emission frequency. The trajectories may be stretched and shifted in height but the topology of the burst remains the same.
The difference in polarization degree between type III (moderate) and spikes (strong) may indicate another emission frequency for the spikes than occurs for the type III burst (e.g. fundamental for spikes and harmonic for type III). This would shift the spike source to lower altitudes with respect to the type III burst without changing the burst topology. The analysis of Benz et al. (1996) shows that the spikes correlate with the extrapolated type III burst to higher frequencies (i.e. the spike frequency). In case of significantly different emission frequencies for spikes and type III burst, a systematic time offset would be expected.
A common feature of all analyzed events (Figs. 3, 4 and 6) is a bending in East – West direction of the trajectories towards the line of sight to the observer, independent of the location on the solar disc. In North – South direction the data also exhibit non-radiality, but no general trend of deviation was observed. Besides this result being an indication for curved magnetic field structures, there are propagation effects that could produce an apparent bending of the magnetic field lines:

- Refraction in the corona can shift the apparent source location.
- The radio emission may be scattered in the corona during propagation to the observer and therefore can produce an apparent image of the source at a location different from the true position (Arzner & Magun 1999 and references therein).
- Type III emission may be beamed along the trajectory of the electrons, selecting only those type III bursts propagating towards the observer within the beaming cone (Caroubalous et al. 1974; Caroubalous & Steinberg 1974).

All events have been analyzed by overlaying EIT images, as shown in Fig. 7 for the 92/08/18 event with an SXT image. Comparable indications of magnetic field structures have been found that can explain at least part of the shift of the projected type III positions towards the observer by the guiding magnetic field. E.g., on 00/05/29, the only other event near central meridian, the observed configuration is consistent with sources in an open flux tube that is anchored in the leading part of the active region as seen by EIT and is part of the field lines which project northward onto the disk. Projection effects make association with active regions difficult in the event of 00/06/20. Nevertheless, the radio sources on 00/06/21 have virtually the same north-south coordinate at all frequencies, and the more they are shifted to the east, the lower the frequency. This is expected for an east-westward extending flux tube anchored in the leading part of the underlying active region, and this interpretation is consistent with the EIT image.
We thus believe that the observations lend plausibility to the assumption that the radio source positions are mainly affected by the magnetic field structure and to a lesser extent by propagation effects. This conclusion is also supported by the work of Pick & van den Oord (1990) and references therein.

5.2. Spike location and acceleration

To inject electrons on the field line guiding the type III burst, the acceleration region must be located close to or on the field line itself. Fig. 9 displays a sketch depicting possible locations of acceleration with respect to a type III burst (A) and a spike source. A priori, there are three different positions for the acceleration region consistent with the present observations: it lies between the type III burst and the spike source (case I), below the spike source (case III) or coincides with the spike source (case II). Assuming that the spike emission is caused by the same acceleration event, location I can be excluded by analyzing spectral radio observations. For the acceleration region to lie in

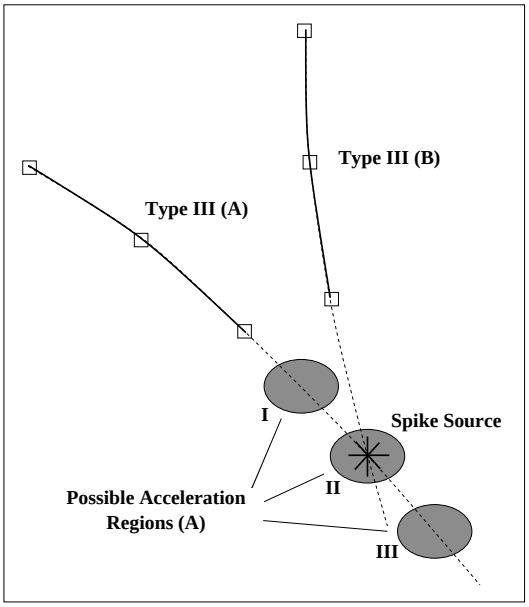

Fig. 9. Sketch of possible locations of the acceleration region (I, II, III) with respect to a type III burst (labeled A) and an associated spike source (asterisk). A second type III (labeled B) is displayed in case of two simultaneous bursts.

between the type III and the spike source, the time of the actual acceleration must lie within the time interval defined by the intersection of the extrapolated type III with the spike frequency and the start of the type III emission. A systematic time delay of the spike source with respect to the acceleration event must be observed, caused by the travel distance of the electrons generating the spike emission. According to Benz et al. (1996) the spikes correlate with the intersection of the extrapolated type III and the spike frequency itself and no systematic delay was found. This analysis supports locations II and III as potential region of acceleration and excludes location I in Fig. 9.
The situation of two type III bursts (labeled A and B in Fig. 9) associated with a single spike source, as was found in two of the 92/08/18 events, suggests location II as a possible acceleration region. Position III is only consistent if the field lines meet in position II and continue in parallel to position III.

6. Conclusions

In all analyzed events the spike sources are always located at positions coinciding with expected locations from extrapolated type III trajectories to lower altitudes. These observations thus strongly support a model for radio spikes occurring in the course of type III beam propagation or near its origin, consistent with independent spectrogram observations (Benz et al. 1996). They add further evidence for spikes being a signature of the mechanism accelerating electron beams that cause type III bursts. This appears to be the simplest interpretation (cf. Fig. 9).

This property is supported by the results of the 92/08/18 observations, where in two events simultaneous or consecutive type III bursts on different magnetic field lines originated in the same spike source. Energetic electrons appear to be injected into different and diverging coronal structures from one single position. Such a diverging magnetic field geometry is the standard ingredient of reconnection. These observations are consistent with the hypothesis that metric spikes may be a signature of particle acceleration. Earlier imaging investigations on metric spikes associated with type III bursts and their interpretation (Krucker et al. 1995; Krucker et al. 1997) can now be compared to these additional observations. They proposed a scenario of energy release at high altitude with up- and downward moving energized electrons. The upward moving electrons produce type III bursts while propagating along open field lines and the downward moving part loses its energy to the lower corona, transition region or upper chromosphere. The radio emission of electron beams moving downward from coronal acceleration sites has occasionally been detected (e.g. Klein et al. 1997), but no signature was seen in the observations presented here. High-sensitivity observations are necessary to investigate the processes below the spike source, i.e. above the spike frequency band.

Acknowledgements. We thank Christian Monstein, Michael Arnold and Peter Messmer (ETH Zurich) for helping to run the Phoenix-2 observations. The evaluation of the Phoenix spectrograms was made using software developed by A. Csillaghy. The work at ETH Zurich is financially supported by the Swiss National Science Foundation (grant No. 2000-061559.00).
The Nançay Radio Observatory is funded by the French Ministry of Education, the CNRS and the Région Centre.

References

Allen, C. W. 1947, MNRAS, 107, 426
Arzner, K., Magun, A. 1999, A&A, 351,1165
Aschwanden, M.J. 1990, A&AS, 85, 1141
Aschwanden, M.J., Güdel, M. 1992, ApJ, 401, 736
Baumbach, S. 1937, Astronomische Nachrichten, 263, 120
Bastian, T.S. 1995, ApJ, 439, 494
Benz, A.O., Kane, S.R. 1986, Solar Physics, 104, 179
Benz, A.O., Csillaghy, A., Aschwanden, M.J. 1996, A&A, 309, 291
Benz, A.O., Zlobec, P., Jaeggi, M. 1982, A&A, 109, 305
Caroubalous, C., Steinberg, J.L. 1974, A&A, 32, 245
Caroubalous, C., Poquérusse, M., Steinberg, J.L. 1974, A&A, 32, 255
Güdel, M., Benz, A.O. 1990, A&A, 231, 202
Güdel, M., Wentzel, D.G. 1993, ApJ, 415, 750
Güdel, M., Zlobec, P. 1991, A&A, 245, 299
Güdel, M.,Aschwanden, M.J., Benz, A.O. 1991, A&A, 251,285
Holman, G.D., Eichler, D., Kundu, M.R. 1980, In: Radio Physics of the Sun, Kundu M.R. and Gergeley T.E. (eds.), IAU Symp., Vol. 86, 457
Kerdraon, A., Delouis, J.-M. 1996, The Nançay Radioheliograph. In: Coronal Physics from Radio and Space Observations, Trottet G. (ed.), Springer Verlag, Berlin, 192

Klein K.-L., Aurass H., Soru-Escaut I., et al. 1997, A&A, 320, 612 (Erratum with correctly printed figures in A&A 322, 1027)
Krucker, S., Aschwanden, M.J., Bastian, T.S., et al. 1995, A&A, 302, 551
Krucker, S., Benz, A.O., Aschwanden, M.J. 1997, A&A, 317, 569
Lang, K. R. 1980, Astrophysical Formulae, Springer-Verlag, Second and enlarged Edition
Leka, K.D., Canfield, R.C., McClymont, A.N., et al. 1996, ApJ, 462, 547-560.
Melrose, D.B., Dulk, G.A. 1982, ApJ, 447, 844
Messmer, P., Benz, A.O. 1999, A&A, 354, 287
Messmer, P., Benz, A.O., Monstein, C. 1999, Solar Physics, 187 (2), 335
Pick M., van den Oord G.H.J. 1990, Solar Physics, 130, 83
Robinson, P.A. 1991, Solar Physics, 134, 299
Suzuki, S., Dulk, G.A. 1985, Bursts of type III and type V, In: Solar radiophysics, McLean D.J. & Labrum N.R. (eds.), Camebridge University Press, 289
Tajima, T., Benz, A.O., Thaker, M., et al. 1990, ApJ, 353, 666
The Radioheliograph Group 1993, Adv. Space Res., 13(9), 411
Trottet, G., Pick, M., House, L., et al. 1982, A&A, 111, 306
Vlahos, L., Sharma, R.R., Papadopoulos, K. 1983, ApJ, 275, 374
Wright, C.S. 1980, Astronomical Society of Australia, Proceedings, 4(1), 62
Zheleznyakov, V.V., Zaitsev, V.V. 1975, A&A, 39, 107